Influence of the solid titanium source on the activity of La1–xTixFeO3 photo-CWPO catalysts under UV-A light

Patricia Garcia-Muñoz, Fernando Fresno, Christophe Lefevre, Didier Robert, Nicolas Keller

Influence of the solid titanium source on the activity of $La_{1-x}Ti_xFeO_3$ photo-CWPO catalysts under UV-A light

Patricia Garcia-Muñoz,*[1,2] Fernando Fresno,[3,4] Christophe Lefevre,[5] Didier Robert, [1] and Nicolas Keller*[1]

1. Institut de Chimie et Procédés pour l'Energie, l'Environnement et la Santé (ICPEES) CNRS/University of Strasbourg, 25 rue Becquerel, Strasbourg, France
2. Universidad Politécnica de Madrid (UPM), E.T.S de Ingenieros Industriales, Departamento de Ingeniería Química Industrial y del Medio Ambiente, c/José Gutiérrez Abascal 2, 28006, Madrid, Spain
3. Photoactivated Processes Unit, IMDEA Energy Institute. Avda. Ramón de la Sagra, 3, Parque Tecnológico de Móstoles, 28935 Móstoles (Madrid), Spain
4. Instituto de Catálisis y Petroleoquímica, CSIC, C/ Marie Curie 2, 28049 Madrid, Spain.
5. Institut de Physique et de Chimie des Matériaux de Strasbourg (IPCMS), CNRS/University de Strasbourg, 23 rue du Loess, Strasbourg, France

* corresponding authors: Patricia Garcia-Muñoz: patricia.gmunoz@upm.es – Nicolas Keller : nkeller@unistra.fr

ABSTRACT

In the search for more efficient low-temperature catalysts able to oxidise biorecalcitrant pollutants in water, the selective substitution of La^{3+} by Ti^{3+} cations was reported to boost the UV-A light driven activity of $LaFeO_3$ orthoferrites as H_2O_2-mediated photo-CWPO catalysts. $La_{1-x}Ti_xFeO_3$ catalysts with $0 < x < 0.11$ were obtained by a modified Pechini sol–gel route via the addition of a solid source of titanium during the synthesis. By using a span of crystallized and amorphous TiO_2, the influence of the titanium source on the substitution rate in the orthoferrite network and on the performances of the catalysts under UV-A light was demonstrated using the degradation of 4-chlorophenol as test reaction.

The amorphous content of the TiO_2 precursor is proposed to be the key factor driving the substitution of La^{3+}, the largest substitution of 11% being obtained using a dried sol-gel TiO_2 precursor. We suggest that the substitution proceeds during the thermal treatment via a solid-solid diffusion between TiO_2 and the amorphous $LaFeO_3$ before it crystallises. The catalyst robustness was influenced by the TiO_2 nature. Small size Ti-$LaFeO_3$ crystallites strongly lowered or blocked the Fe release, while no improvement was observed for large size crystallites vs. the pristine material, what was associated to a poor homogenization of the titanium in the network. We showed that the mineralization activity was proportional to the substitution rate of $La_{1-x}Ti_xFeO_3$ catalysts, while a similar relationship could be drawn for the degradation activity only in the case of highly robust catalysts with pure heterogeneous surface reactions.

KEYWORDS: dual Ti-substituted $LaFeO_3$ catalyst ; photoassisted CWPO ; photocatalysis ; advanced oxidation processes ; water treatment

1. INTRODUCTION

The increase in the amounts of polluted water and the existence of refractory pollutants in the water streams prompt the search for new processes able to meet the regulations and the legislation requirements in force, and to reach the necessary abatement of the biorecalcitrant pollutants [1]. Advanced Oxidation Processes (AOPs) have shown their ability to oxidise recalcitrant pollutants of water that are not removed by conventional treatments, through the generation of $HO_x^\bullet$ radicalar species that can stepwise oxidise the organic matter up to CO_2 and H_2O [2-4]. There is a vast classification of AOPs combining O_3, O_2, UV, H_2O_2 and/or a catalyst into a wide span of processes such as photocatalysis, ozonation, Fenton or photo-Fenton processes (or their heterogenous counterparts as CWPO and photo-CWPO, respectively), etc.

Photocatalysis and CWPO-like processes have received attention due to their efficiency and low cost. Though photocatalysis can achieve full mineralization of a wide spectra of dissolved pollutants, it suffers from low reaction rates and UV-light dependence for the most active TiO_2 references. Also photo-CWPO takes advantage of higher reaction rates, but does not reach complete mineralization. Combining both AOPs in a single light-driven catalyst is thus considered as a worth approach for synergistically benefitting from their advantages and overcoming their respective drawbacks [4-7].

$LaFeO_3$ is a versatile material that has been employed as catalyst in different AOPs at dark and illuminating conditions [8-11]. It is a p-type semiconductor with a narrow band gap value (between 2.1- 2.7 eV) and a orthoferrite (distorted) perovskite (ABO_3) structure, whose main characteristic is that the B cation presents redox properties associated to the oxygen mobility, and that develops redox surface activity. Further, its properties and in particular its redox properties can be modified by a controlled (partial) replacement of the A or B cations [7-10, 12, 13]. In photocatalysis or photo-Fenton catalysis, works on the partial cationic A (La) or B (Fe) sub-lattice substitution of the $LaFeO_3$ perovskite remain scarce, notably in comparison to the wide span of heteroatom-doped TiO_2 systems studied. The removal of organic dyes in water by photocatalysis was improved via the partial substitution of La by Li [14] or Ca, or that of Fe by Zn or Mn [15]. Some works were reported in heterogeneous photo-

Fenton catalysis under visible or UV-A light, targeting dyes, methylparaben micropollutant or acetic acid [16,17]. Substitution with cations with different radii, valence-electron numbers and coordination numbers was notably reported to enhance the redox activity by producing electron-deficient or electron-rich species at the surface [18].

Our precursor work first showed the high-prospect capability of a single-phase Ti-substituted $LaFeO_3$ orthorferrite material to behave as a dual light-driven catalyst able to take advantage of a synergistic effect between heterogeneous photo-Fenton catalysis and photocatalysis under UV-A light [7]. It generates HO_x° radicals by Fe-catalyzed H_2O_2 decomposition under UV-A light (photo-CWPO), while simultaneously showing photocatalytic activity thanks to its semiconductor nature with a suited band gap and well-located electronic bands. Photocatalysis was proposed here to allow the cleaning of the catalyst surface from poisoning Fe-carboxylate complex intermediates blocking the mineralization and leading to Fe leaching to the aqueous medium. The catalyst was prepared by means of a simple modified Pechini sol–gel route via the addition of a solid source of Ti heteroatom during the synthesis.

The partial substitution of La by Ti ions stabilised in the state 3+ in the A-site of the orthoferrite network was demonstrated by XRD analysis with Rietvelt structural refinement and XPS surface analysis [19,20]. It enhanced both the catalyst performances and its robustness compared to the pristine $LaFeO_3$, as full mineralization of 4-chlorophenol (4-CP) as model pollutant was achieved under UV-A light, with improved degradation and mineralization rates and with no loss of activity after 5 test cycles. This was proposed to result from an enhanced photogenerated charge carriers availability at the surface and an electronic enrichment of surface iron. We however reported that the nature of the Ti precursor might impact the properties of the catalyst and thus its behavior in water treatment [19,21].

Therefore, this work aimed at studying the influence of the Ti precursor source on the performances of dual Ti-modified $LaFeO_3$ catalysts under UV-A light. To this end, a set of commercially available TiO_2 and an amorphous TiO_2 sample were selected as solid precursors, and the removal of

the 4-chlorophenol (4-CP) under UV-A light was used as test reaction, as a example of industrial waste water refractory pollutant.

2. MATERIALS AND METHODS

2.1 Materials

Reactants for synthesis and photocatalytic reactions were used as purchased from Sigma-Aldrich: H_2O_2 (>30%), $La(NO_3)_3 \cdot 6H_2O$, $Fe(NO_3)_3 \cdot 9H_2O$, citric acid hydrate ($C_6H_8O_7 \cdot xH_2O$, 99.5%), titanium tetraisopropoxide (TTIP, 97%) and 4-Cl-Phenol (>99%). NH_3 (30% aqueous solution) was obtained from Carlo Erba. Aeroxide© TiO_2 P25 and Aeroxide© TiO_2 P90 were provided by Evonik. TiO_2 UV100 Hombikat was obtained from Sachtleben Chemie GmbH while TiO_2 CristalACTiVE PC500 was provided by Tronox.

2.2 Synthesis of Ti-modified $LaFeO_3$

$La_{1-x}Ti_xFeO_3$ catalysts were synthesised by a modified Pechini sol-gel route. $La(NO_3)_3 \cdot 6H_2O$ (108.3 g/L) and $Fe(NO_3)_3 \cdot 9H_2O$ (133 g/L) in stoichiometric ratio were dissolved in deionised water (30 mL), and the metal ions were subsequently complexed by adding the stoichiometric amount of citric acid (70 g/L). For the synthesis of the catalysts labelled as P25-LFO, P90-LFO, UV-LFO and PC-LFO, Ti was included by incorporating Aeroxide© TiO_2 P25, Aeroxide© TiO_2 P90, UV100 Hombikat and PC500, respectively, into the starting ferrite sol under vigorous stirring, in a quantity equivalent to 10 wt.% with respect to the theoretically obtained amount of $LaFeO_3$. The resultant suspensions were heated up to 80 °C with a 2 °C min^{-1} ramp and kept at this temperature for 48 h for a total gelification to be attained. The dry gel was calcined with the heating cycle described by Gosavi et al. [22], namely heating up with a ramp of 5 °C min^{-1}, keeping the temperature at 600 °C for 2 h, and then reaching a second plateau at 800 °C for 2 h.

For the synthesis of the SG-LFO catalyst, a laboratory-made dried amorphous TiO_2 was used as source of titanium. This TiO_2 was prepared by means of a sol-gel procedure in alkaline conditions using TTIP as precursor. Typically, 17.8 g of TTIP was initially poured into 40 mL of ethanol, and then the

same volume of water was added dropwise. Aqueous NH_3 was adedd until a pH of 9 was reached, and then the solution was kept at room temperature under stirring until a dry paste resulted, which was dried further at 110 °C for 12 h to finally obtain the amorphous titania used in the procedure described above.

Keeping the titanium dopant apart, the stoichiometry of the reaction leading to the formation of $LaFeO_3$ orthoferrite is represented by Eq.1 [23]:

$$La(NO_3)_3x6H_2O + Fe(NO_3)_3x9H_2O + C_6H_8O_7xH_2O \rightarrow LaFeO_3 + 6CO_2 + 3N_2 + nH_2O \quad \text{[Eq.1]}$$

Unmodified lanthanum ferrite, referred to as LFO, was obtained with the same procedure without adding titania and used as reference material.

2.3. Characterisation techniques

X-ray diffraction (XRD) patterns were recorded using a Bruker D8 Advance equipment with a monochromated copper X-ray source (K_α = 1.54056 Å), in θ/θ mode and with a scan step of 0.02°. Fullprof software was used for Rietveld refinement, where the line shape of the diffraction peaks was created using the modified Thompson-Cox-Hasting function. Instrumental peak width was determined by measuring the scattering of corundum (NIST standard SRM 1976b) [24,25]. The mean crystallite size (average size of the coherent diffracting domains) was estimated with the Scherrer equation using the full patterns after refinement, assuming sphere-shaped crystallites as usually done and considering instrumental broadening.

Surface areas were determined from nitrogen adsorption isotherms, measured with a Micrometrics Tristar 3000 equipment at −196 °C after outgassing the samples at 250°C for 16 h.

The metal contents were determined by ICP-OES (inductively coupled plasma optical emission spectroscopy) with an Optima 7000 DV equipment from Perkin Elmer.

Fluorescence lifetimes were determined by time-correlated single photon counting (TCSPC) in a

Mini-τ equipment (Edinburgh Instruments). An EPL375 laser diode (445.2 nm, 90.7 ps pulse width, 1 MHz repetition rate) was used as excitation source. A band pass filter at 600 ± 25 nm was positioned between the sample and the detector.

2.4. Reaction procedure

4-chlorophenol degradation experiments were performed in batch-mode in a borosilicate glass beaker reactor under atmospheric pressure. The temperature was kept constant at 20 ± 2 °C with a thermostated bath. Typically, 100 mL of an aqueous 4-CP solution (25 mg L^{-1}, equivalent to 14.8 ppm total organic carbon) were placed in the reactor and then the catalyst (50 mg, 0.5 g L^{-1}) was added and kept dispersed with vigorous magnetic stirring in the dark for 1h to allow the adsorption/desorption equilibrium to be attained. H_2O_2 was then added in an amount equivalent to the stoichiometric concentration for complete mineralization of the initial pollutant, i.e. 125 mg L^{-1}. Irradiation was then provided by Philips 24W/10/4P UV-A lamps (60 W/m^2; λ_{max}=365 nm). During the reaction, samples (8 mL) were taken from the reactor at regular intervals by means of a syringe and filtered using a 0.2 μm membrane filters to remove the catalyst powder. The decay of the concentration of 4-CP was followed by keeping track of the intensity of the absorption peak at λ= 224 nm [26] in the filtered samples by means of a UV-vis spectrophotometer (VWR UV-1600 PC). Additionally, the total organic carbon (TOC) content of the filtered samples was measured with a Shimadzu TOC-L analyzer. The Fe leached into the reaction medium during the reaction was quantified by using the ortho-phenanthroline method, as described in Supporting Information S1 [27].

3. RESULTS AND DISCUSSION

3.1. Catalyst characterization

Figure S1 shows the XRD patterns of the unmodified and different Ti-modified $LaFeO_3$ catalysts, as well as their Rietveld refinement profiles. The XRD patterns of LFO displays the diffraction peaks of the

(110), (112), (022), (220), (312) and (224) planes of the $LaFeO_3$ phase (JCPDS card 070–7777) at 2θ = 22.6, 32.2, 39.7, 46.1, 57.4 and 67.3, respectively. A small fraction of α-Fe_2O_3 (11%) with a mean crystallite size of 35 nm was observed as an additional phase (JCPDS card 033-06664). Regardless of the employed source of titanium, all the patterns of the Ti-modified $LaFeO_3$ samples can be indexed to the Pbnm orthorhombic unit cell of $LaFeO_3$, with no significant variation regarding the α-Fe_2O_3 additional phase. Neither La_2O_3 nor TiO_2 are detected as extra phases. ICP-OES analysis reveals the atomic titanium content in the Ti-containing $LaFeO_3$ catalysts ranging from 2.9% when prepared using the P90-TiO_2 precursor up to 4.0% for the amorphous TiO_2 nanopowder (Table 1). The cation distribution in the $LaFeO_3$ structure from Rietveld refinements, as well as the crystallographic data, are collected in Table S1 and S2, respectively.

Depending on the heteroatom atom nature, substitution has been evidenced on both the A and the B sites of the $LaFeO_3$ structure, although cations in a high oxidation state usually substitute and locate in the Fe^{3+} sites [28,29]. However, many external factors have been shown to influence the cation substitution in oxides (like the synthesis temperature or the cooling rate) [30,31], and no empirical rules related to steric or electronic criterion drive the location of the heteroatom. Refinement of both Ti/La and Ti/Fe site occupations demonstrated that Ti atoms were located preferentially in the lanthanum A site and substituted only the La atoms, independently of the titanium source. Considering a $La_{1-x}Ti_xFeO_3$ labelling with *x* being the partial Ti→La substitution rate for La atoms in the A-site, the substitution rate within the orthoferrite structure was 5, 6, 7 and 8 at.% for the P25-TiO_2, PC500-TiO_2, UV100-TiO_2, P90-TiO_2 precursors, respectively, and increased up to 11 at.% for the dried TiO_2 precursor (Tables 1 and S1).

The TiO_2 precursors used differ notably regarding crystalline phases (anatase and anatase/rutile mixture), crystallinity, crystallite size and specific surface area, and their main physico-chemical properties are listed in Table 1. The phase composition refers only to the crystalline TiO_2 phases, while the amorphous content was estimated by means of the method described in [32]. It is worth noting that the partial x substitution rate was found to be related to the amorphous content of the precursor

used: the higher the amorphous content, the higher the substitution rate, as evidenced in Figure 1 top. Using the fully amorphous sol-gel TiO_2 as solid source of titanium atoms led to get the highest substitution rate of 11 at.%. We can therefore propose that the partial Ti→La substitution proceeds in the course of the thermal treatment through a solid-solid diffusion between TiO_2 and the amorphous $LaFeO_3$ before it crystallises. The atomic titanium diffusion into the amorphous $LaFeO_3$ network is proposed to be favoured by the amorphous nature of the solid TiO_2 precursor, what in consequence would increase the substitution rate. Differences in terms of specific surface areas for the $La_{1-x}Ti_xFeO_3$ catalysts might result from the relative ratio between the kinetic of crystallization of the LFO structure and that of the diffusion of titanium atoms.

It must be said that the band gap of the catalysts is not affected by the substitution rate within the LFO structure, as the band gap was graphically estimated at 2.04 ± 0.04 eV from the Tauc plots derived from UV-vis diffuse reflectance spectra regardless of whether the catalyst is doped or not, and the Ti precursor source used (Figure S2).

The fluorescence decays of the different catalysts is shown in Figure 1 bottom. In comparison to the pristine $LaFeO_3$ sample, a slower decay was observed for the Ti-substituted $La_{1-x}Ti_xFeO_3$ catalysts, irrespective of the Ti source used and the substitution rate. Using a bi-exponential function, the fluorescence lifetimes were calculated as the average of both parameters [21]. Considering that the fluorescence emission results from transitions from surface electronic states, the higher fluorescence lifetime observed for the $La_{1-x}Ti_xFeO_3$ catalysts can be associated to a longer lifetime of the electrons trapped in these states, that characterises slower radiative recombination kinetics and in consequence an enhanced availability of photogenerated charges for reacting with adsorbed species [33,34]. The SG-LFO catalyst exhibited by far the longest fluorescence lifetime, associated to an enhanced charge separation. However, no straightforward relationship could be established between the lifetime of charges and the substitution rate. First, the crystallite size can have an impact on the carrier lifetime and thus should be considered. For a similar LFO crystallite size, the higher the amount of substituting titanium, the lower the recombination rate, as it is observed when comparing SG-LFO and P25-LFO

with crystallite sizes of 20-21 nm. Second, we cannot rule out an indirect role of the additional α-Fe_2O_3 minority phase through the formation of a type-II (staggered) $La_{1-x}Ti_xFeO_3$/α-Fe_2O_3 heterojunction, both valence and conduction bands of the α-Fe_2O_3 being more anodic than the corresponding bands of the ferrite after Fermi level alignment [35]. Although beneficial charge transfer might occur in this model for improving charge separation, no direct correlation was established between the wt.% content of additional α-Fe_2O_3 phase and the fluorescence lifetime.

Table 1. Main physico-chemical properties of the solid TiO_2 precursor, the pristine $LaFeO_3$ and the Ti-substituted $LaFeO_3$ catalysts.

Catalyst	TiO_2 precursor properties					Ti-substituted LFO ($La_{1-x}Ti_xFeO_3$)				
	TiO_2 nature	BET surface of TiO_2 precursor	TiO_2 phase composition (A/R) [a]	Anatase crystallite size (nm) [b]	Amorphous phase content (%) [c]	Substitution rate *x* (at.%)	Fe (at.%)	Ti (at%)	S_{BET} (m^2/g)	Mean crystallite size of LFO (nm)
LFO	-	-	-	-	-	-	23.0	-	8	46
P25-LFO	P25	51	80/20	22	7	5	16.0	3.2	28	21
P90-LFO	P90	90	90/10	13	29	8	15.0	2.9	70	27
UV-LFO	UV100	330	100/0	9	26	7	19.4	4.0	19	41
PC-LFO	PC500	336	100/0	7	20	6	21.0	4.0	17	37
SG-LFO	amorphous sol-gel	- [d]	amorphous	-	100	11	22.7	4.0	5	20

[a] the phase composition corresponds to the composition within the crystallised TiO_2 phases (without considering the content of amorphous TiO_2). A and R represent the anatase and rutile phase, respectively

[b] determined by applying the Scherrer equation to the (101) and (110) peaks of anatase and rutile, at 25.7° and 27.5°, respectively.

[c] determined by using the method developed in ref [31]

[d] cannot be determined as the outgassing under vacuum modifies the properties of the dried sol-gel TiO_2 precursor

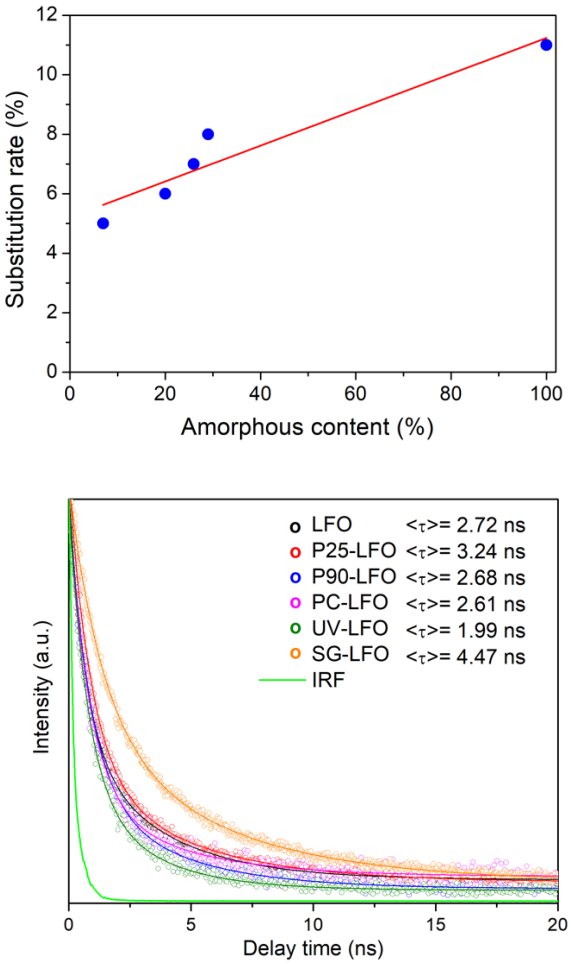

Figure 1. (top) Influence of the TiO_2 amorphous content on the partial Ti→La substitution rate (*x*) in La A-site within the orthoferrite $La_{1-x}Ti_xFeO_3$ structure ; **(bottom)** Fluorescence decay curves of the unmodified $LaFeO_3$ and different Ti-substituted $La_{1-x}Ti_xFeO_3$ catalysts. The lines correspond to the bi-exponential curves fitted to each set of experimental data. <τ> stands for the average fluorescence lifetime. IRF: instrument response function (IRF).

3.2. Catalytic activity

The catalytic behaviour of the full series of Ti-modified $La_{1-x}Ti_xFeO_3$ catalysts has been evaluated and compared to that of the pristine titanium-free $LaFeO_3$ counterpart. Control experiments confirmed that no photolysis was observed under UV-A light, and that both LFO and Ti-modified LFO catalysts do not show any activity in absence of UV-A light and of H_2O_2. The activity of the catalysts in CWPO in the dark is shown in Figure S3. Figure 2 shows the evolution with UV-A irradiation time of both 4-CP concentration and TOC amount during the H_2O_2-mediated photocatalytic reaction, together with that of the Fe released. While the reference $LaFeO_3$ catalyst was able to remove the 4-CP pollutant within 150 min, it did not fully mineralise the effluent and reached a maximum TOC conversion of 75%, with reference kinetic rate constants for 4-CP and TOC conversions of 0.020 min^{-1} and 0.12 mg L^{-1} min, respectively. It must be said that the reference LFO catalyst suffered from important Fe leaching to the aqueous solution, with a Fe released value of 0.5 mg/L being detected in water after 120 min of test.

By contrast, the full series of $La_{1-x}Ti_xFeO_3$ catalysts allowed to reach complete mineralization in 90 to 120 min of reaction, with enhanced kinetic rate constants in the 0.17-0.28 mg/Lmin range. The substituted catalysts degrade the 4-CP substrate within shorter times than the pristine catalyst, namely within the 60-120 min range, with enhanced kinetic rate constants in the 0.025-0.042 min^{-1}.

The Fe leaching during the reaction was also influenced by the nature of the TiO_2 precursor used in the modified Pechini synthesis. The leaching observed for both UV-LFO and PC-LFO catalysts was similar to that observed for the pristine LFO catalyst, namely around 0.5-0.6 mg/L, but it strongly decreased to 0.05 mg L^{-1} for both P25-LFO and P90-LFO catalysts, and further down to undetectable values in the experiment with the SG-LFO catalyst. In consequence, direct correlation between the kinetic rate constant for 4-CP degradation and the substitution rate cannot be drawn, as the high amount of Fe leached during the reactions with the pristine LFO and with both UV-LFO and PC-LFO

catalysts can significantly contribute to the $k_{4\text{-}CP}$ value calculated, through a classical homogeneous photo-Fenton reaction. By contrast, in the case of the P25-LFO, P90-LFO and SG-LFO catalysts, the $k_{4\text{-}CP}$ values derived from experimental data could be assumed not to include any homogeneous photo-Fenton reaction, as those catalysts are characterised by a low (or the absence of) Fe release. So, in the case of pure heterogeneous surface reactions, Figure 3A reveals that the higher the substitution rate, the higher the kinetic rate constant for the 4-CP degradation. It must be said that the $k_{4\text{-}CP}$ values calculated in the case of a, in agreement with a significant contribution of free Fe species in solution.

The kinetic rate constant for TOC removal is assumed to be less dependent on the amount of Fe released to the reaction medium, as the homogeneous Fe species are forming complexes with short-chain carboxylic acids, consequently not contributing to a significant extent to the mineralization rate constant. Therefore, a direct relationship between the substitution rate of the $La_{1-x}Ti_xFeO_3$ catalysts and the k_{TOC} was established, and revealed that the higher the Ti → La substitution value, the higher the kinetic rate constant for mineralization (Figure 3B).

As above-mentioned, we cannot completely rule out the indirect role played by a $La_{1-x}Ti_xFeO_3$/α-Fe_2O_3 heterojunction through an improved charge separation, however we assume that this is not a predominant factor driving the activity of the catalysts, as no correlation was established between the wt.% content of additional α-Fe_2O_3 phase, the fluorescence lifetime and the catalytic indicators.

Increasing the amorphous content of the solid titanium source is an elegant way to increase the cationic substitution rate of La by Ti atoms, and in consequence to increase the amount of electron-enriched surface Fe that boost the photo-CWPO activity. However, some substituted catalysts did not show an improved robustness in terms of Fe release to the solution compared to the pristine LFO system (UV-LFO and PC-LFO). This might be associated to a poor homogenization of the titanium inside the network that resulted in large LFO crystallite size (37-41 nm), as a strongly enhanced robustness was observed for lower-size LFO crystallites (P25-LFO, P90-LFO, SG-LFO).

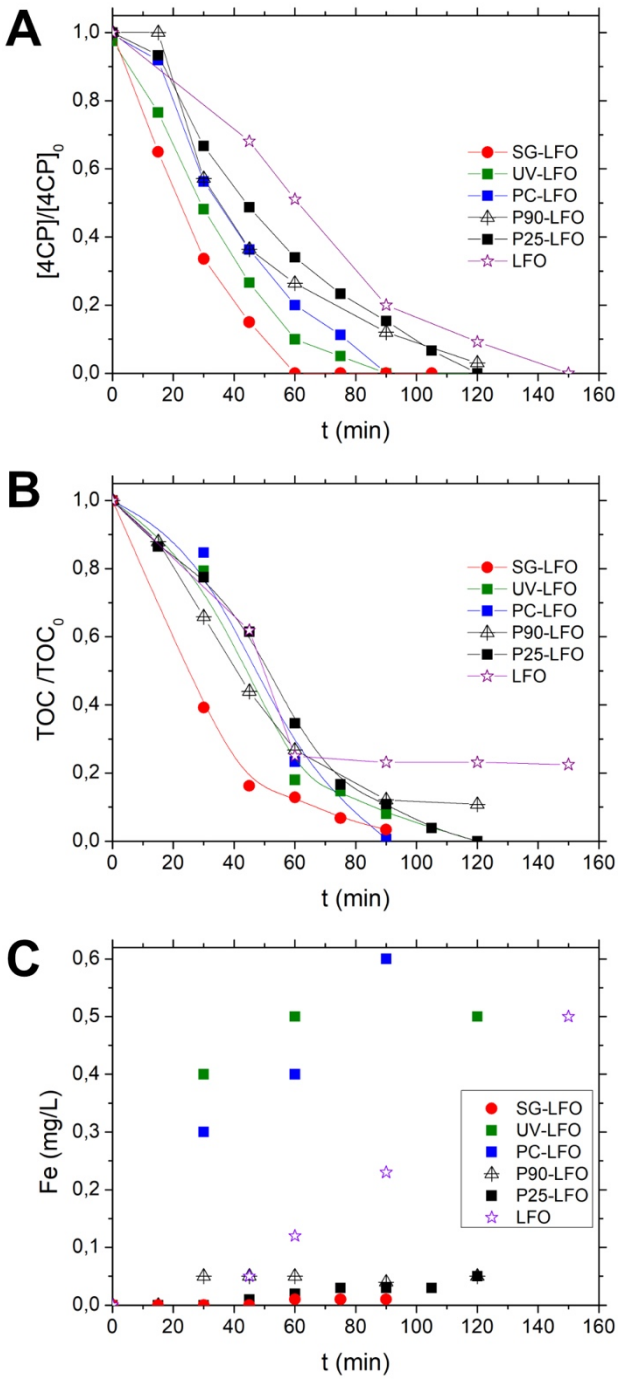

Figure 2. Evolution of **(A)** the relative 4-CP concentration, **(B)** the relative TOC concentration and **(C)** the concentration of Fe released during the photoassisted CWPO process with the different Ti-substituted $La_{1-x}Ti_xFeO_3$ catalysts under UV-A light compared to unmodified $LaFeO_3$.

Table 2. Kinetic rate constants of 4-CP oxidation and TOC mineralization, TOC conversion achieved after 120 min, and iron leached to the solution.

Catalyst	k' (4-CP) (min^{-1})[a]	$r_{0\ TOC}$ (mg/Lmin)[b]	X_{TOC} (120 min)	$Fe_{leached}$ (mg/L)
LFO	0.020	0.12	75	0.5
P25-LFO	0.025	0.18	100	0.05
P90-LFO	0.030	0.20	100	0.05
UV-LFO	0.040	0.19	100	0.5
PC-LFO	0.033	0.18	100	0.6
SG-LFO	0.042	0.28	100	<0.001[c]

[a] a pseudo first-order kinetic was used as usually admitted for fitting the 4-CP concentration evolution curves

[b] a zero-order kinetic model was used as usually admitted for fitting the TOC concentration evolution curves

[c] the detection limit of Fe leached to the solution has been measured at 0.001 ppm.

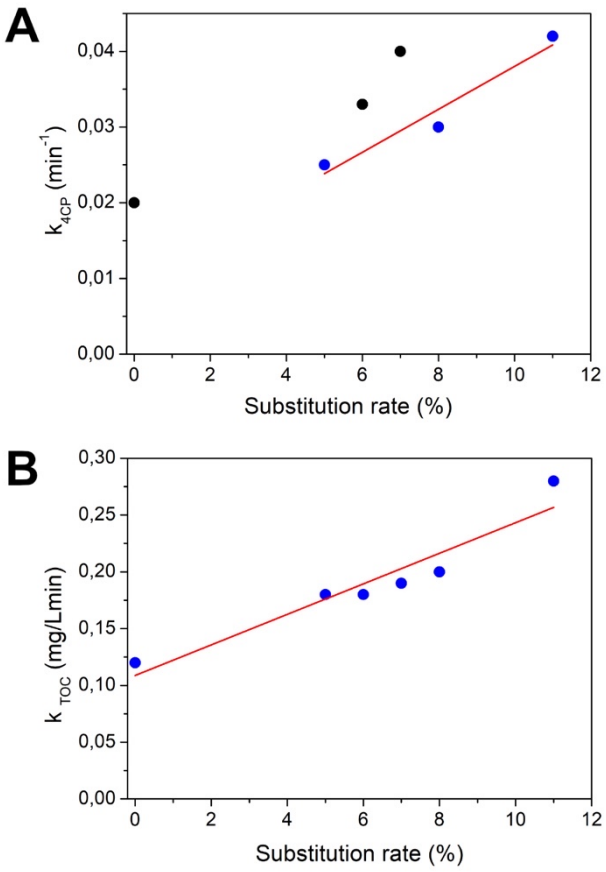

Figure 3. Influence of the substitution rate x on the kinetic rate constants of **(A)** 4-CP oxidation ($k_{4\text{-}CP}$) and **(B)** TOC mineralization (k_{TOC}) obtained using the $La_{1-x}Ti_xFeO_3$ catalysts under UV-A light. In (A), the blue marks correspond to $k_{4\text{-}CP}$ values assumed not to contain any significant homogeneous photo-Fenton contribution due to the absence of (or the very low) Fe release to the aqueous media.

4. CONCLUSION

We have shown that the selective substitution of La^{3+} by Ti^{3+} cations is a promising way to increase both activity and robustness of $LaFeO_3$ orthoferrites as H_2O_2-mediated photo-CWPO catalysts for the removal of biorecalcitrant pollutants in water. Controlled cationic substitution was achieved through the addition of a solid source of titanium during a facile citric acid-based Pechini sol-gel synthesis with final thermal treatment at 800°C. The amorphous content of the TiO_2 precursor was reported to be the key-factor driving the substitution of La^{3+} in the orthoferrite network, the use of a dried sol-gel TiO_2 precursor allowing to reach the largest substitution rate of 11% in the $La_{1-x}Ti_xFeO_3$ catalysts in comparison to more crystallized titanium sources. We proposed that the substitution proceeds in the course of the thermal treatment via a solid-solid diffusion between TiO_2 and the amorphous $LaFeO_3$ before it crystallizes.

We showed that the performances of the $La_{1-x}Ti_xFeO_3$ catalysts under UV-A light in the removal of 4-chlorophenol in water can be related to the substitution rate in the orthoferrite network. We evidenced that the mineralization kinetic is proportional to the substitution rate, while a similar relationship can be drawn in regards to the degradation kinetic for the high-robustness $La_{1-x}Ti_xFeO_3$ catalysts that operate only via pure heterogeneous surface reactions without any significant photo-Fenton reaction contribution in homogeneous phase. Indeed, the nature of the TiO_2 used as titanium source influenced also the robustness of the substituted catalysts by impacting on the size of the resulting $La_{1-x}Ti_xFeO_3$ crystallites. Small size crystallites were proposed to strongly lower or block the

Fe release, while no improvement was observed for large size crystallites vs. the pristine material, what was associated to a poor homogenization of the titanium in the network.

Acknowledgements

The European Fund for regional development (EFRE/FEDER) is thanked for funding the project PHOTOPUR in the frame of Interreg V program and Offensive Sciences call. PGM acknowledges Comunidad de Madrid through the call Research Grants for Young Investigators from Universidad Politécnica de Madrid for funding the research project SUNCAT4PLAST (APOYO-JOVENES-21-JV4DEB-3-Q2WGKV) investigadores.

REFERENCES

[1] T.T.N. Phan, A.N. Nikoloski, P.A. Bahri, D. Li, Heterogeneous photo-Fenton degradation of organics using highly efficient Cu-doped LaFeO3 under visible light, Journal of Industrial and Engineering Chemistry. 61 (2018) 53-64.

[2] N. Serpone, Y.M. Artemev, V.K. Ryabchuk, A.V. Emeline, S. Horikoshi, Light-driven advanced oxidation processes in the disposal of emerging pharmaceutical contaminants in aqueous media: A brief review, Current Opinion in Green and Sustainable Chemistry. 6 (2017) 18-33.

[3] S. Malato, P. Fernández-Ibáñez, M.I. Maldonado, J. Blanco, W. Gernjak, Decontamination and disinfection of water by solar photocatalysis: Recent overview and trends, Catalysis Today. 147 (2009) 1-59.

[4] G. Pliego, J.A. Zazo, P. Garcia-Muñoz, M. Munoz, J.A. Casas, J.J. Rodriguez, Trends in the Intensification of the Fenton Process for Wastewater Treatment: An Overview, Crit. Rev. Environ. Sci. Technol. 45 (2015) 2611-2692.

[5] P. García-Muñoz, G. Pliego, J.A. Zazo, A. Bahamonde, J.A. Casas, Sulfonamides photoassisted oxidation treatments catalyzed by ilmenite, Chemosphere. 180 (2017) 523-530.

[6] G. Pliego, P. Garcia-Muñoz, J.A. Zazo, J.A. Casas, J.J. Rodriguez, Improving the Fenton process by visible LED irradiation, Environ. Sci. Pollut. Res. (2016) 1-7.

[7] P. Garcia-Muñoz, C. Lefevre, D. Robert, N. Keller, Ti-substituted LaFeO3 perovskite as photoassisted CWPO catalyst for water treatment, Applied Catalysis B: Environmental. 248 (2019) 120-128.

[8] Y. Rao, F. Han, Q. Chen, D. Wang, D. Xue, H. Wang, S. Pu, Efficient degradation of diclofenac by LaFeO3-Catalyzed peroxymonosulfate oxidation---kinetics and toxicity assessment, Chemosphere. 218 (2019) 299-307.

[9] F. Parrino, E. García-López, G. Marcì, L. Palmisano, V. Felice, I.N. Sora, L. Armelao, Cu-substituted lanthanum ferrite perovskites: Preparation, characterization and photocatalytic activity in gas-solid regime under simulated solar light irradiation, Journal of Alloys and Compounds. 682 (2016) 686-694.

[10] Y. Song, S. Xue, G. Wang, J. Jin, Q. Liang, Z. Li, S. Xu, Enhanced photocatalytic decomposition of an organic dye under visible light with a stable LaFeO3/AgBr heterostructured photocatalyst, Journal of Physics and Chemistry of Solids. 121 (2018) 329-338.

[11] S. Afzal, X. Quan, J. Zhang, High surface area mesoporous nanocast LaMO3 (M=Mn, Fe) perovskites for efficient catalytic ozonation and an insight into probable catalytic mechanism, Applied Catalysis B: Environmental. 206 (2017) 692-703.

[12] K. Peng, L. Fu, H. Yang, J. Ouyang, Perovskite LaFeO3/montmorillonite nanocomposites: synthesis, interface characteristics and enhanced photocatalytic activity, Scientific Reports. 6 (2016) 19723.

[13] H. Wang, Z. Guo, W. Hao, L. Sun, Y. Zhang, E. Cao, Ethanol sensing characteristics of BaTiO3/LaFeO3 nanocomposite, Materials Letters. 234 (2019) 40-44.

[14] L. Hou, G. Sun, K. Liu, Y. Li, F. Gao, Preparation, characterization and investigation of catalytic activity of Li-doped LaFeO3 nanoparticles, J. Sol Gel Sci. Technol. 40 (2006) 9-14.

[15] Z. Wei, Y. Wang, J. Liu, C. Xiao, W. Zeng, Synthesis, magnetization and photocatalytic activity of LaFeO3 and LaFe0.5Mn0.5−xO3−δ, Materials Chemistry and Physics. 136 (2012) 755-761.

[16] D. Sannino, V. Vaiano, P. Ciambelli, L.A. Isupova, Structured catalysts for photo-Fenton oxidation of acetic acid, Catal. Today 161 (2011) 255–259.

[17] C. Orak, S. Atalay, G. Ers.z, Photocatalytic and photo-Fenton-like degradation of methylparaben on monolith-supported perovskite-type catalysts, Sep. Sci. Technol. 52 (2017) 1310–1320.

[18] K. Pan, H. Hou, J. Hu, J. Yang, J. Xiang, C. Li, C. Xu, S. Chen, S. Liang, J. Yang, Ca and Cu doped LaFeO3 to promote coupling of photon carriers and redox cycling for facile photo-Fenton degradation of bisphenol A, Chemosphere. 308 (2022) 136325.

[19] P. García-Muñoz, F. Fresno, C. Lefevre, D. Robert, N. Keller, Synergy Effect Between Photocatalysis and Heterogeneous PhotoFenton Catalysis on Ti-Doped LaFeO3 Perovskite for High Efficiency Light-Assisted Water Treatment, Catal. Sci. Technol. (2020).

[20] P. García-Muñoz, F. Fresno, C. Lefevre, D. Robert, N. Keller, Ti-Modified $LaFeO_3$/β-SiC Alveolar Foams as Immobilized Dual Catalysts with Combined Photo-Fenton and Photocatalytic Activity, ACS Appl. Mater. Interfaces 12 (2020) 57025.

[21] P. Garcia-Muñoz, F. Fresno, C. Lefevre, D. Robert, N. Keller, Highly robust La1-xTixFeO3 dual catalyst with combined photocatalytic and photo-CWPO activity under visible light for 4-chlorophenol removal in water, Applied Catalysis B: Environmental. 262 (2020) 118310.

[22] P.V. Gosavi, R.B. Biniwale, Pure phase LaFeO3 perovskite with improved surface area synthesized using different routes and its characterization, Mater. Chem. Phys. 119 (2010) 324-329.

[23] X. Qi, J. Zhou, Z. Yue, Z. Gui, L. Li, A simple way to prepare nanosized LaFeO3 powders at room temperature, Ceramics International. 29 (2003) 347-349.

[24] L.B. McCusker, R.B. Von Dreele, D.E. Cox, D. Louër, P. Scardi, Rietveld refinement guidelines, J. Appl. Cryst. 32 (1999) 36-50.

[25] J. Rodríguez-Carvajal, Recent advances in magnetic structure determination by neutron powder diffraction, Physica B: Condensed Matter. 192 (1993) 55-69.

[26] M. Pera-Titus, V. García-Molina, M.A. Baños, J. Giménez, S. Esplugas, Degradation of chlorophenols by means of advanced oxidation processes: a general review, Applied Catalysis B: Environmental. 47 (2004) 219-256.

[27] E.B. Sandell, Colorimetric Determination of Traces of Metals, 49 ed., The Journal of Physical Chemistry, 1945.

[28] T.S. Jamil, H.A. Abbas, R.A. Nasr, R.-. Vannier, Visible light activity of BaFe1-xCuxO3-d as photocatalyst for atrazine degradation, Ecotoxicol. Environ. Saf. 163 (2018) 620-628.

[29] S.K. Rashmi, H.S. Bhojya Naik, H. Jayadevappa, R. Viswanath, S.B. Patil, M. Madhukara Naik, Solar light responsive Sm-Zn ferrite nanoparticle as efficient photocatalyst, Materials Science and Engineering: B. 225 (2017) 86-97.

[30] M.R. De Guire, R.C. O'Handley, G. Kalonji, The cooling rate dependence of cation distributions in CoFe2O4, J. Appl. Phys. 65 (1989) 3167-3172.

[31] Z.J. Zhang, Z.L. Wang, B.C. Chakoumakos, J.S. Yin, Temperature Dependence of Cation Distribution and Oxidation State in Magnetic Mnâˆ'Fe Ferrite Nanocrystals, J. Am. Chem. Soc. 120 (1998) 1800-1804.

[32] L. Cano-Casanova, A. Amorós-Pérez, M. Ouzzine, M.A. Lillo-Ródenas, M.C. Román-Martínez, One step hydrothermal synthesis of TiO2 with variable HCl concentration: Detailed characterization and photocatalytic activity in propene oxidation, Applied Catalysis B: Environmental. 220 (2018) 645-653.

[33] A. Charanpahari, S.S. Umare, S.P. Gokhale, V. Sudarsan, B. Sreedhar, R. Sasikala, Enhanced photocatalytic activity of multi-doped TiO2 for the degradation of methyl orange, Appl. Catal. A Gen. 443–444 (2012) 96–102.

[34] R.S. Varma, N. Thorat, R. Fernandes, D.C. Kothari, N. Patel, A. Miotello, Dependence of photocatalysis on charge carrier separation in Ag-doped and decorated TiO2 nanocomposites, Catal. Sci. Technol. 6 (2016) 8428–8440.

[35] N. Zhang, S. Ruan, Y. Yin, F. Li, S. Wen, Y. Chen, Self-Sacrificial Template-Driven $LaFeO_3$/α-Fe_2O_3 Porous Nano-Octahedrons for Acetone Sensing, ACS Appl. Nano Mater. 2018, 1(9) (2018) 4671–4681